# Modelling the structure of Zr-rich $Pb(Zr_{1-x}Ti_x)O_3$, $x$=0.4 with a multiphase approach

Alexander Bogdanov,[1,2] Andrey Mysovsky,[1,2] Chris Pickard,[3,4] and Anna V. Kimmel[5,6]

[1] *Vinogradov Institute of Geochemistry SB RAS, 1a Favorsky Street, Irkutsk, 664033, Russia*
[2] *Irkutsk National Research Technical University, 83 Lermontov Street, Irkutsk, 664074, Russia*
[3] *Department of Materials Science and Metallurgy, University of Cambridge, 27 Charles Babbage Road, CB3 0FS UK*
[4] *Advanced Institute for Materials Research, Tohoku University, 2-1-1 Katahira, Aoba, Sendai, 980-8577, Japan*
[5] *National Physical Laboratory, Hampton Road, Teddington TW11 0LW, UK*
[6] *Department of Physics and Astronomy, University College London, Gower Street, London WC1E 6BT, UK**

(Dated: September 17, 2016)

Solid solution perovskite $Pb(Zr_{1-x}Ti_x)O_3$ (PZT) is an industrially important material. Despite the long history of experimental and theoretical studies the structure of this material is still under intensive discussion. In this work we have applied structure searching coupled with Density Functional Theory methods to provide a multiphase description of this material at $x$=0.4. We demonstrate that the permutational freedom of B-site cations leads to the stabilisation of a variety of local phases reflecting the relatively flat energy landscape of PZT. Using a set of predicted local phases we reproduce the experimental pair distribution function (PDF) profile with a high accuracy. We introduce a complex multiphase picture of the structure of PZT and show that additional monoclinic and rhombohedral phases account for better description of the experimental PDF profile. We propose that such a multiphase picture reflects the entropy reached in the sample during preparation process.

PACS numbers: 77.84.-s,77.80.Fm

## INTRODUCTION

Complex perovskite solid solution materials, such as $A(BB')O_3$ and $AA'(BB')O_3$, are of great interest for actual or potential uses, based on their exceptional piezoelectric properties. A family of solid solution perovskites with high piezo-response find use in great variety of devices such as nonvolatile random-access memory (NVRAM), dynamic random-access memory (DRAM), micro-electromechanical systems (MEMS), high performance piezoelectric MEMS including transducers, actuators, micro-pumps, inkjet printheads, and pyroelectric detectors [1–7].

Among these materials lead zirconate titanate, $Pb(Zr_{1-x}Ti_x)O_3$ (PZT), is a disordered solid solution $ABO_3$ perovskite material, with Pb ion at the A-site, while Ti and Zr cations are randomly distributed over the B-sites. Permutational freedom of B-site cations, along with rotational degrees of freedom of the $BO_6$ octahedra, gives rise the variety of stable phases in PZT, which is apparent in its complex temperature-composition phase diagram [8–14]. The Ti-rich side of the PZT phase diagram exhibits tetragonal symmetry at low temperatures, while the Zr-rich side displays a complex behaviour. At $x$ <0.03 the system exhibits an antiferroelectric (AFE) phase that disappears with the increase of the Ti content and the solid solutions adopt rhombohedral symmetry [15]. The border separating tetragonal and rhombohedral phases (around 48-52 % of Ti content) is referred to morphotropic phase boundary (MPB).

The origin of the MPB in solid solution systems, such as PZT, is of great interest from both, fundamental science and industrial points of view, due to the possibility of engineering compounds with exceptional and controlled properties. The generally accepted model of the MPB in PZT is related to the appearance of monoclinic phase in a narrow compositional range around MPB [8]. This provides a mechanism to transform from a rhombohedral to tetragonal phase through a common monoclinic subgroup ($Cm$). The latter explains the freedom of the lead cations to move within the mirror plane of the monoclinic phase, and, thus, enhance the polarisation rotation and piezo-response [8, 16, 17].

The role of lead-displacements on the short-range order was found to be significant, while the order of Ti and Zr cations considered to have random homogeneous arrangement exhibiting similar ferroelectric displacements [18, 19].

The analysis of distribution of cation-displacements is usually attributed to the appearance of low symmetry phases and has been performed in number of works [12, 13, 18–21], while there is lack of information on the arrangements of B-site cations due to the limit of the resolution of the technique.

A strong effect of composition on the distribution of the directions of lead displacements was described in ref. [20], indicating the dominance of [100] pseudo-cubic lead displacements for Ti-rich local environment, while Zr-rich environment tends to accommodate [110] displacements.

It was shown that Ti and Zr cations adopt different displacements within their octahedral environments, although determination of displacements was at the limit of the resolution of the technique [18]. The results indicated

an off-centre polar displacement for Ti in agreement with the findings from nuclear magnetic resonance (NMR) results [22, 23], however, it found nearly zero displacement for Zr.

High field NMR measurements have shown great promise as a probe of the local structure of $ABO_3$ perovskite-based alloys. NMR solid-state study of PZT demonstrated non-random character of B-site cations distribution with the presence of Ti-O-Ti chains along the (001) plane on the local scale [23].

The role of cation displacements in short- and long-range structural order of PZT has been discussed in ref. [12], where authors proposed a gradual change in the range of order as a means to develop individual phases, rather than distinct long-range structures separated by sharp phase boundaries.

Several low-symmetry phases were predicted for PZT in MPB region shortly after the discovery of $Cm$ phase. Authors of ref. [24] predicted three monoclinic, so-called $M_a$, $M_b$, $M_c$, phases and a triclinic phase using high-order Devonshire theory [25].

Recently, the short-range scale structural complexity of PZT and its relationship to the piezo-activity has been discussed [13]. The authors discussed the nature of the monoclinic phase across the Zr-rich area of morphotropic phase boundary of PZT and found coexisting long-range average rhombohedral and both long- and short-range monoclinic regions.

The study of local and average structures of PZT is of fundamental importance in understanding the origin of its high-performance piezoelectricity. Understanding the motifs of local structure provides an insight into the relationship between the microscopic changes in local structure and macroscopic composition-driven properties.

In this work we describe the structure of $Pb(Zr_{1-x}Ti_x)O_3$, $x$=0.4 in vicinity of MPB using multiphase approach. Assuming that a solid solution material is composed of small nano-regions with correlated ferroelectric displacements and B-cation arrangements, we describe its structure as a set of distributed nanoscale local phases.

Using a set of local phases predicted by the random structure search technique coupled with the Density Functional Theory methods[26] we reproduce the experimental pair distribution function (PDF) profile with high accuracy [13, 27]. We show that permutation of B-site cations leads to stabilisation of a variety of local phases with characteristically different lead displacements. Our results demonstrate that Zr-rich PZT exhibits a complex multiphase structure predominate rhombohedral structure at long-range order, while constituted of low-symmetry areas on a local scale.

## METHODS

The study of disordered solid solution compounds such as PZT from first-principles is a challenging task due to the statistical gap between relatively small DFT-accessible systems and the disorder imposed by B-site cation arrangements in real material. However, quenched disorder in B-cation arrangements in PZT makes the approach based on the analysis of local structure well suited for structural studies of this material [28].

To bridge the statistical gap in this work we have performed structure sampling of $Pb(Zr_{1-x}Ti_x)O_3$ in perovskite stoichiometry region using AIRSS (*"Ab-initio"* Random Structure Searching) technique [29, 30]. Successfully applied to a variety of systems [30, 31], AIRSS generates a large ensemble of structures, each of which has a reasonable starting volume and interatomic distances. Application of this method is particularly advantageous for potential energy surface sampling of such a complex compound with established polymorphism as PZT.

To sample the energy landscape of ferroelectric perovskite compound we have strongly biased the AIRSS algorithm to preserve $ABO_3$ topology. The searches have been performed for a number of configurations with inequivalent arrangements of B-site cations. We sampled the potential energy surface of cells containing 8 formula units simultaneously varying arrangements of Ti and Zr cations, lattice parameters, ferroelectric displacements and octahedral tilting angles.

The statistical analysis of DFT-predicted structures of PZT at MPB-composition has been performed in ref. [28], where it was shown that B-site cations arrangement is a crucial factor for the chemistry of the PZT. In the present work we significantly extended the statistics of probed PZT configurations - AIRSS generated several thousands of structures over the range of compositions.

Despite unambiguous data on B-site cations distribution in PZT the use of relatively small DFT-cells is consistent with the conclusions made in ref. [32], where the mean cluster size distribution for Zr and Ti was estimated. It was shown that the sum of the mean clusters as a function of composition reaches its minimum in the vicinity of MPB enclosing a volume of about 20.25 PZT unit cells, which corresponds roughly to a cube with an edge length of about 11 Å. Assuming such a homogeneity in B-cation distribution the diameter of clusters of PTO or PZO should be comparable with $2 \times 2 \times 2$ unit cell system (8 Å).

We have performed the structure search for end-members of PZT diagram that correspond to pure PZO and PTO compounds as well as number of Ti- and Zr-rich compositions with $x$=0.25, 0.375, 0.5, 0.625 and 0.75.

To distinguish between the types of constructed PZT structures we used following notations: each type of B-

cations arrangement was denoted with roman superscript index. Thus, with composition $x$=0.5 a cell containing four Ti and four Zr cations can be represented by six symmetry inequivalent arrangements. As such, the arrangement $0.5^{I}$ corresponds to the ordering of B-site cations of the same type in staggered columns collinear to one of the <100> crystallographic directions; the arrangement $0.5^{II}$ represents rock-salt-type ordering of B-cations, which corresponds to the inversion operation applied to the centre of the cell with permutation of the B-cations; arrangements $0.5^{III-V}$ are related to an asymmetric non-uniform clustering of B-cations, where Zr and Ti ions occupy planes perpendicular to one of the <100> directions in proportion of 3:1 (i.e. one Zr and three Ti atoms per atomic plane); the arrangement $0.5^{VI}$ corresponds to the ordering of the same type B-cations within a layer lying in a {100} crystallographic plane. Similar notations were used for other probed compositions: $x$=0.25, $x$=0.375, $x$=0.625, $x$=0.75. For all compositions the arrangement of type $I$ corresponds to the structure with Ti (or Zr) atoms occupying a {100} plane. The arrangement $II$ corresponds to location of Ti (or Zr) atoms in {110} plane, while the variant $III$ corresponds to Ti (or Zr) cations in {111} without clustering.

Each constructed structure was fully relaxed within the Density Functional Theory level using PBEsol exchange-correlation functional [33] as implemented in the VASP code [34–37]. The projector augmented wave pseudopotentials [38–40] with 550 eV energy cutoff and $6 \times 6 \times 6$ Monkhorst-Pack $k$-points mesh per formula unit were chosen. The convergence of the total energy and forces during optimisation were of 1 meV and 0.01 eV/Å, respectively. The potential energy landscape is probed at zero K, thus, in this work we do not discuss the effects of anharmonicity or temperature effects.

The macroscopic polarisation, $P$, has been esimtaed through the sum of the products of the atomic displacements and Born effective charges [41]. The latter as well as the components of the piezoelectric tensor were calculated using linear response approach as implemented in the VASP code [42–44].

An important descriptor for the atomic structure of a material is the pair distribution function (PDF), $g(r)$, which determines the probability of finding two atoms at a given distance, $r$. Experimentally, the pair distribution function $g_t(r)$ is derived from measured (by X-Ray or neutron experiment) structure factor of a material. Computationally, the function $g_m(r)$ is calculated from the distributions of atomic centres corresponding to the modelled structure. We assume that a solid solution material is composed of small nano-scaled regions with correlated ferroelectric displacements and B-cation arrangements, that can be described as a set of distributed local phases. To identify the type of local phase that is presented in real materials and provide a contribution to the experimental structural data profile we developed a fitting procedure that approximates the target pair distribution function, $g_t(r)$, i.e. experimental structural data, with a modelled pair distribution function $g_m(r)$. The function $g_m(r)$ is constructed as a linear combination of PDFs from local structures predicted by structure search technique (further denoted as *optimisation set*):

$$g_m(r) = \sum_j C_j \; g_j(r, L_j^k, \sigma_j)$$

Here $g_j(r, L_j^k, \sigma_j)$ is the PDF of the $j$-th local structure and $C_j$ is the linear combination coefficient which corresponds to the contribution weight of this local structure into the target function. The summation over index $j$ runs over all DFT-simulated structures including all probed stoichiometries. Coefficients $L_j^k$ (where $k = 1, 2, 3$) stand for lattice parameters of the $j$-th local structure, while the variable $\sigma_j$ scales the ferroelectric displacements of the $j$-th structure.

The optimisation of $L_j^k, \sigma_j$ parameters is done to account for thermal effects, plausible deformations and effects of local electric fields arising from surrounding domains with different polarisation directions. The lattice parameters were allowed to vary within 4 % of the DFT-calculated values with symmetry constraints. The variables $\sigma_j$ were allowed to modify ferroelectric displacements of the $j$-th structure within 20 % of that calculated by DFT. Independent to $L_j^k$ variation of $\sigma_j$ imposes an additional degree of freedom on variation of B-O bond lengths within 0.1 Å.

The fitting procedure consists of minimising the deviation between target, $g_t$, and modelled, $g_m$ functions:

$$\delta S = \frac{\sum_p (g_t(r_p) - g_m(r_p))^2}{\sum_p (g_t(r_p))^2},$$

where $r_p$ is the uniform mesh of distances between 0 and $r_{max}$. In other words, fitting of $g_m$ to $g_t$ is done in the range from 0 to $r_{max}$.

For construction of stereographic projection for a pseudo-cubic perovskite we calculate the vector of cation displacements from [111] direction for each local phase, identifying a direction with a tolerance of 0.04 Å. Thus, each vector is represented at the projection as a point with a colour gradient reflecting a relative contribution to the displacement direction.

## RESULTS AND DISCUSSION

### *Ab Initio* Structure Search

We performed the analysis of the potential energy landscape of PZT at ambient pressure using *ab initio* random structure search [26]. As an initial step we performed sampling of the PES of well-known

$PbTiO_3$(PTO) and $PbZrO_3$(PZO) compounds. We found tetragonal $P4mm$ structure to be the most stable PTO phase with lattice parameters of $a$=3.87 Å, $c$=4.17 Å that are in good agreement with experiment [20]. The tetragonal phase is followed by 0.09 eV less stable cubic $Pm\bar{3}m$ phase with a computed 0 K lattice parameter of 3.92 Å.

Our searches also correctly predict the phase stability of PZO: the most stable phase is found to be antiferroelectric $Pbam$ structure with the lattice parameters $a$=5.89 Å, $b$=11.82 Å, $c$=8.19 Å in good agreement with experiment [45] that is followed by 0.38 eV less stable paraelectric $Pm\bar{3}m$ phase with $a$=4.15 Å lattice parameter in good agreement with earlier simulations [46, 47].

Further, we have sampled the potential energy landscape of PZT compounds with different compositions of $x$=0.25, 0.375, 0.5, 0.625, 0.75. Despite sampling over relatively small cells we have obtained a variety of stable phases from monoclinic to cubic symmetry. Notably, the greatest range of phases within a given arrangement was found at near-to-MPB compositions – relaxation of the six inequivalent arrangements $0.5^{I-VI}$ has converged to 38 stable different symmetry phases. Meanwhile, searches for compositions $x$=0.375, 0.625 have converged to 13 and 9 different phases, respectively and for compositions $x$=0.25, $x$=0.75 - to 9 and 11 phases, respectively.

The diversity of phases confirms the flatness of the potential energy landscape in vicinity of MPB and suggests that phase coexistence region is confined close to the composition $x$=0.5 rather than extended to wide range of concentrations.

Estimating the relative energy of a solid solution phase as:

$$dE = E_{PbZr_{1-x}Ti_xO_3} - [x\ E_{PbTiO_3} + (1-x)\ E_{PbZrO_3}],$$

we plot the relative energies of phases found in Fig. 1b for each composition and each arrangement type. As we show later, structures with maximal contribution to the experimental PDF curve are marked by red diamonds denoting weight and the symmetry. We have found that the potential energy landscape of PZT is characterised by a relatively flat profile – most of our phases lie within a 0.09 eV energy interval, which is consistent with the conclusions of earlier work [48].

We note that phases with different composition may exhibit a very similar stability that makes them competitive in solid solution compound.

### Fitting procedure

To justify the applicability and performance of our fitting procedure we have performed several tests to reproduce pair distribution function for well defined tetragonal and cubic phases of PTO. For this we constructed a target function, $g_t^{t-PTO}(r)$, using the parameters of tetragonal phase refined from neutron scattering experiments [20] for PTO at room temperature. To probe the robustness of our method we have included into the optimisation set predicted by the structure search tetragonal phase of PTO, antiferroelectric phase of PZO, and all found PZT structures – overall, 82 structures.

Our technique has successfully fitted $g_m^{t-PTO}(r)$ to the target function with relative error $\delta S$ of 0.023. The model function $g_m^{t-PTO}(r)$ contained 99 % of tetragonal PTO with parameters $a$= 3.90, $c$=4.15 Å, while 1 % is related to erroneous determination of paraelectric phase of PZT with $0.5^{II}$ arrangement (Fig. 2a). We have also tested our fitting procedure to reproduce the PDF profile of the cubic phase of PTO. We used similar to the tetragonal case optimisation set with enhanced scaling of lattice and ferroelectric parameters that cover centrosymmetric atomic positions and cubic lattice parameters. Despite the large difference between structural parameters of cubic and tetragonal phases, our fitting procedure reproduced $g_t^{c-PTO}(r)$ (Fig. 2b) with high accuracy (the relative error $\delta S$ is of 0.029). The modelled function $g_m^{c-PTO}(r)$ consists of 98 % of PTO with the lattice parameters and ferroelectric distortion close to the cubic phase values: $a$= 3.90 Å, while the parameter $\sigma$ has converged to zero that correspond to the absence of ferroelectric displacements. Our procedure, however, provides an erroneous 1.5 % contribution of a tetragonal lattice, which we consider as an accuracy of our method.

Further we apply our approach to describe the phase composition of PZT with $x$=0.4. As a target function $g_t^{PZT}(r)$ we have used PDF, which was obtained as a Fourier transform of the structure factor of PZT [13, 27]. The data was collected at room temperature by the neutron scattering experiment for ceramic samples of PZT with composition of $x$=0.4 prepared by mixed oxide route.

We used 82 structures in the optimisation set that included pure PTO, PZO compounds and all predicted PZT structures at various composition. Optimising the set of variables $C_j$, $\sigma$, $L_j^i$ we have successfully obtained model function $g_m^{PZT}(r)$ that matches the target curve $g_t^{PZT}(r)$ with high accuracy – the relative error is only 0.025. This compare to 0.023 and 0.029 error related to tetragonal and cubic PTO cases, respectively (Fig. 2). The model function $g_m^{PZT}(r)$ reproduced the experimental curve over the wide range of distances (up to 50 Å) including short- and long-range intervals (Fig. 3).

Notably, our 82 structures set has converged to a subset containing only 10 structures (further called *final set*) with non-zero coefficients $C_j$. Final set does not contain any contribution from pure PTO and PZO compounds ($x$=0, 1), and Ti-rich configurations with $x$=0.625, 0.75. The maximal contribution of 25 % belongs to the monoclinic structure $Pm$ related to

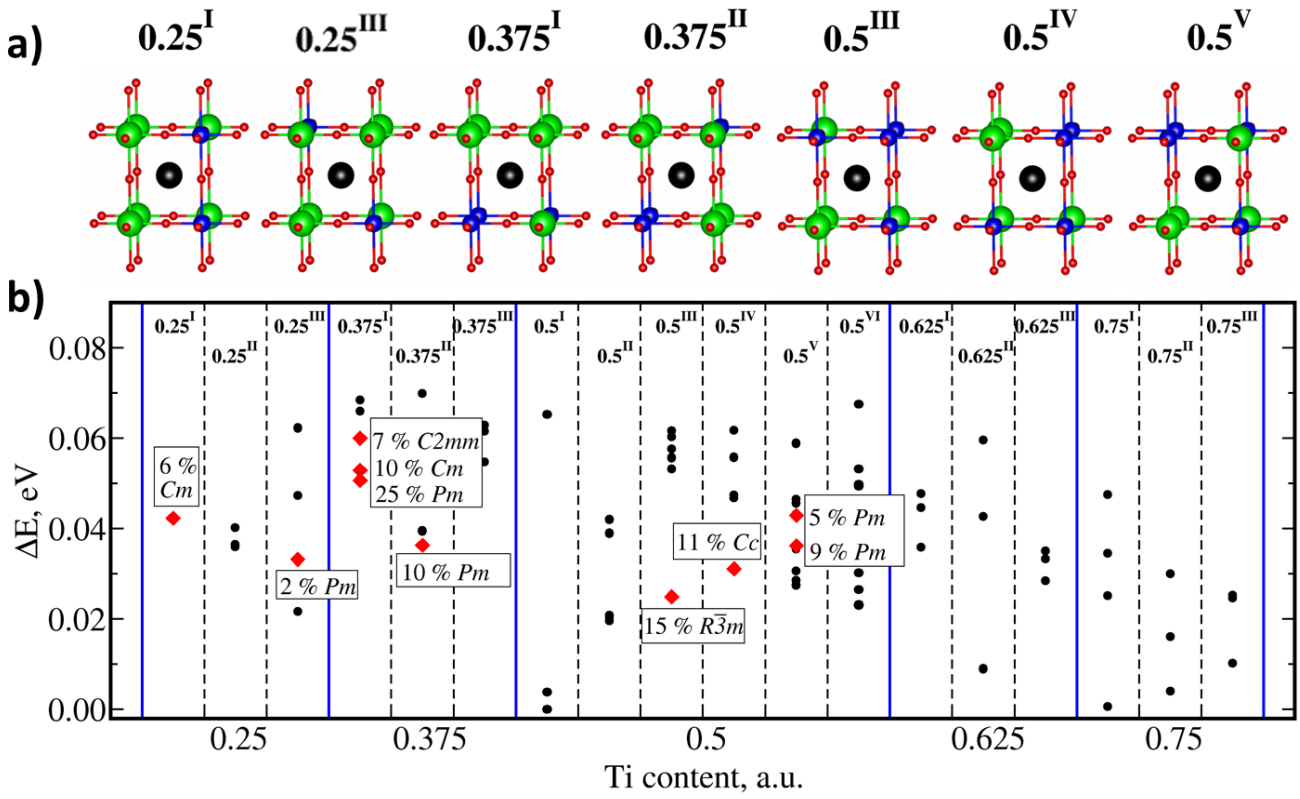


Figure 1. (Color online) Local phases of PZT and their relative stabilities. a) Schematic representation of the arrangements of B-site cations that correspond to local phases selected by the fitting procedure. Ti, Zr, Pb, O atoms are shown by blue, green, black and red spheres, respectively. b) Relative stabilities of PZT local phases obtained by AIRSS for the range of compositions x=0.25, 0.375, 0.5, 0.625, 0.75. For clarity the stabilities of less stable paraelectric structures are not shown. The local phases which contribute to the $PbZr_{0.6}Ti_{0.4}O_3$ model function are marked by red diamonds with local phase symmetry and percentage contribution shown.

$0.375^I$ arrangement (Fig. 1a). High energy structures with identical arrangements, monoclinic $C2mm$ and $Cm$ phases, compose about 17 % of the model function $g_m^{PZT}(r)$. The rest of the curve consists of the structures related to six different arrangements with three distinct compositions: $x$=0.25, 0.375 and 0.5. These contributions vary from 2 % up to 15 % as it shown in Fig. 1b. Notably, only a small part of the converged local structures (8 %) corresponds to the composition $x$=0.25, i.e. mostly deviating from the overall averaged material's composition. One can see that similar stoichometry phases provide smaller contribution to the final set as their stability decreases, which reflects their temperature stability.

Our fitting procedure has also correctly reproduced the sample composition: overall Ti content, $x$, was found to be of 0.42, which is very close to the experimental sample composition of 0.4. We found a strong variation of $x$ among the structures contributing to $g_m^{PZT}(r)$ - only about a half (52 %) of them are condensed within arrangements ($0.375^{I,II}$), i.e. have composition closest to the experimental value of 0.4. Meanwhile, a similar contribution of 48 % belongs to phases with $x$=0.5 and $x$=0.25, i.e. with compositions greatly deviating from $x$=0.4. Such a variation suggests a spatial compositional variation ($\Delta x$) in the experimental sample. Based on compositions of contributing structures, we assume $\Delta x$ not exceeding the value of 0.15.

Interesting to note that some of the contributing structures are characterised by the presence of Ti-O-Ti chains perpendicular to polar direction. This is somehow in agreement with NMR findings, where those chains were shown to preserve in equatorial plane up to high Zr-contents, unlike similar chains in axial direction [23].

The analysis of the mutual arrangement of B-site cations, i.e. population of B-sites by Ti and Zr cations, demonstrates a structural similarity of the phases contributing to the $g_m^{PZT}(r)$. Considering a conversion path between different arrangements as a substitution of Ti by Zr ions at the B-sites (and vice versa), one can count

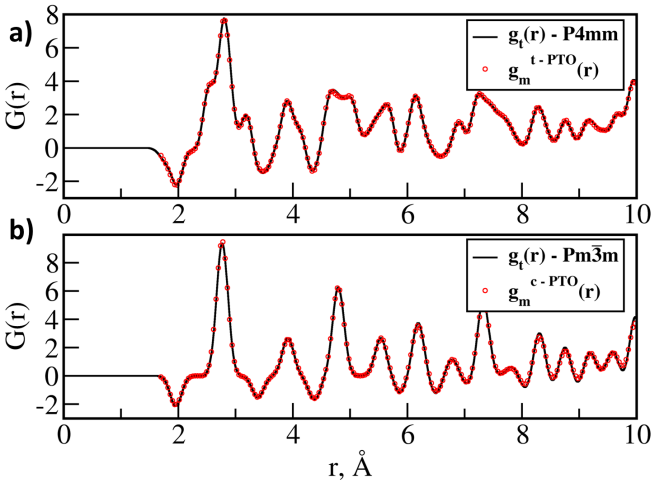


Figure 2. (Color online) Target and modelled pair distribution functions for a) tetragonal phase of $PbTiO_3$. Target function $g_t^{t-PTO}(r)$ shown by black solid curve, while modelled function $g_m^{t-PTO}(r)$ corresponds to red open circles. b) Target ($g_t^{c-PTO}(r)$) and modelled ($g_m^{c-PTO}(r)$) functions for cubic $PbTiO_3$.

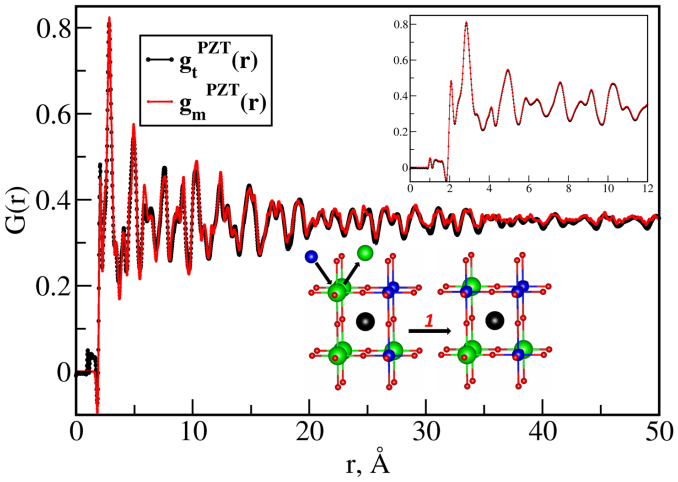


Figure 3. (Color online) Experimental target $g_t^{PZT}(r)$ function and modelled $g_m^{PZT}(r)$ pair distribution functions for Zr-rich $PbZr_{0.6}Ti_{0.4}O_3$. The short-range distances are shown within the insert. Schematics of the conversion path between arrangements $0.375^I$ and $0.5^{III}$ that contribute 47 % and 16 %, respectively

a number of substitution steps required for a conversion between two different arrangements (see Fig. 3). One can see that the structures with largest coefficients $C_j$ are topologically close to the specific arrangement $0.375^I$. In particular, we found that 42 % of the $g_m^{PZT}(r)$ is represented by the arrangement $0.375^I$ itself, while 46 % is composed by $0.5^{III,IV,V}$ and $0.25^I$ arrangements. The latter ones require only one substitution operation to convert to the arrangement $0.375^I$. Finally, only 12 % of $g_m^{PZT}(r)$ is composed by the arrangements $0.375^{II}$ and $0.25^{III}$ that take two and three substitution operations, respectively, to convert to $0.375^I$ arrangement.

During the annealing process a solid solution system maintains its maximal entropy due to the enhanced diffusion of B-site cations that produces a variety of local arrangements. However, the cooling process condensates local minima representing those arrangements into their energy minima which then appear in structure determination experiment. Therefore, our linear combination PDF, $g_m^{PZT}(r)$, represents a set of local minima, which correspond to the maximal entropy of a solid solution system achieved in the sample during the manufacturing process.

Our observations suggest a presence of a long-range *averaged* order in the sample that related to the arrangement $0.375^I$. However, the material is also characterised by some deviations from this long-range order - local short-range structure. We found that the smaller the difference between the *local* and the *averaged* arrangements, the greater the probability for the local arrangement to appear in the sample.

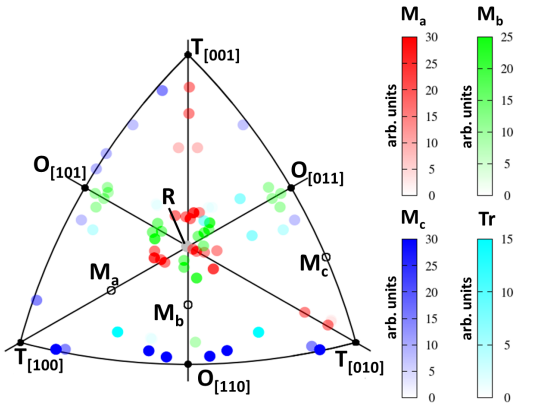


Figure 4. Stereographic [111] projection of lead displacements collected over the local phases contributing to $g_m^{PZT}(r)$. The **T** and **O** points refer to tetragonal and orthorhombic symmetry, respectively. Red, green, blue circles correspond to monoclinic $\mathbf{M}_a$, $\mathbf{M}_b$ and $\mathbf{M}_b$ phases, respectively [24]. Cyan circles correspond to triclinic (**Tr**) phases. The colour gradient shows relative contribution of corresponding displacements in the model structure.

We have performed the analysis of stereographic (111) projection of lead displacements for the local phases that contribute to the $g_m^{PZT}(r)$ function. In Fig. 4 one can see that 5 % of all lead displacements are related to exact **R** symmetry – centre of the graph, meanwhile there is no contribution corresponding to pure **T** or **O** directions. Notably, the majority of lead displacements are roughly equally distributed over several types of mono-

clinic structures: phases $\mathbf{M}_a$, $\mathbf{M}_b$ and $\mathbf{M}_c$ compose 27 %, 26 % and 29 %, respectively. In addition we have found that 12 % of all lead displacements occurs in the triclinic direction.

Overall, our results suggest a diverse character of lead displacements in Zr-rich PZT that would make it difficult to describe the structure of this system by a single- or two-phase model. We, however, highlight that such a diversity of lead displacements is driven by the B-O interactions and relaxation of B-cation sub-lattice, while lead sub-lattice exhibits relative freedom in displacements.

We propose that the structure of Zr-rich PZT can be considered as a set of different symmetry nano-regions characterised by a complex distributions of lead displacements. Such a picture is consistent with the recent diffuse scattering experiments [49] where it was shown that strongly structured diffuse scattering from morphotropic PZT suggests presence of differently ordered local regions.

Our findings are also in line with the consideration made in ref. [13] which suggests that the structure of PZT can be described as a set of local low-symmetry phases, while on the long-range scale the structure exhibits rhombohedral symmetry. Authors of ref. [13] proposed an elegant model of solid solution PZT compound consisting of *microscale* regions, which exhibit monoclinic symmetry at the local scale. Being distributed and oriented randomly these regions in diffraction experiments on average could give **R** structure. However, in the case of correlation between neighbouring regions established up to large enough scales, this leads to the formation of a *macroscopic* monoclinic phase and produces corresponding diffraction peaks.

However, following questions still remain open: *What is the microscopic structure of such correlated regions?* and *What is the physical origin of such correlation?*

The description of the microscopic structure of a correlated region in PZT based on lead displacements analysis could be very complex: local phase forming a nano-region may exhibit a diversity of displacement directions. For example, the local phase $0.5_1^{III}$, which provides 15 % of contribution to $g_m^{PZT}(r)$ function, exhibits the $R\bar{3}m$ symmetry group and $[11\bar{1}]$ polarisation direction. Meanwhile, this 40-atoms local structure has eight lead ions that characterised by six lead ions with $\mathbf{M}_a$ and $\mathbf{M}_b$-type of displacements and two ions with **R**-type displacements directions.

We suggest that the diversity of lead displacements strongly reflects the character of B-cation distribution over the local phase and reflects the chemistry of the compound. The cation displacements are established in order to optimise B-O and A-O bond lengths in highly inhomogeneous structures. This suggests that structural correlations in solid solution materials, which give rise to the ordered nano-regions, are not due to ferroelectric displacements, but are established firstly at the level of B-cation distribution.

### Ferroelectric and piezoelectric properties of PZT structures with maximal coefficients

Further, we have performed the analysis of ferroelectric and piezoelectric properties of local PZT phases contributing to model $g_m^{PZT}(r)$ function to provide an insight into the correlation between these properties and the local order of B-site cations. The calculated values of spontaneous polarisation, $\boldsymbol{P}$, and piezoelectric stress tensor elements, $e_{ij}$ are shown in Table I. We found a strong variation of the magnitude and the direction of polarisation with respect to the local phase. The calculated values of $\boldsymbol{P}$ vary from 0.55 up to 0.74 C/m$^2$, not exceeding though the experimental value 0.75 C/m$^2$ [50] and in good comparison with earlier simulations [51]. In general, we found that the condition for the enhanced $\boldsymbol{P}$ and large ferroelectric distortions is related to the presence of Zr-O-Zr chains oriented along the polar axis. This arrangements causes elongation of the cell, so, Ti-ions in collinear Ti-O-Ti chains adopt large ferroelectric displacements.

The analysis of piezoelectric coefficients $e_{ij}$ (values for $e_{31}$, $e_{33}$ and $e_{15}$ are shown in Table I) demonstrates their strong dependence on the symmetry and structural parameters of the cells and vary from zero up to values of about 7 C/m$^2$. However, we have not found a particularly high piezoelectric response from predicted local phases - calculated piezoelectric constants are comparable with those of pure PTO (Table I). This suggests that the *extrinsic* contributions such as domain wall motion [52] could be responsible for large piezo-activity of PZT rather than effects of local arrangement.

Table I. Calculated electromechanical properties of PZT local structures contributing to $g_m(r)$.

| name | symmetry | P, $C/m^2$ | $e_{31}$, $C/m^2$ | $e_{33}$, $C/m^2$ | $e_{15}$, $C/m^2$ |
|---|---|---|---|---|---|
| $0.25_1^I$ | $Cm$ | 0.73 | 2.4 | 5.3 | 0.5 |
| $0.25_1^{III}$ | $Pm$ | 0.58 | 0.8 | 7.8 | 1.7 |
| $0.375_1^I$ | $Pm$ | 0.65 | 1.3 | 4.9 | 0.9 |
| $0.375_2^I$ | $C2mm$ | 0.72 | 0.0 | 0.0 | 0.0 |
| $0.375_3^I$ | $Cm$ | 0.72 | 2.1 | 5.9 | 0.8 |
| $0.375_1^{II}$ | $Pm$ | 0.74 | 0.1 | 4.4 | 5.0 |
| $0.5_1^{III}$ | $R\bar{3}m$ | 0.55 | 0.8 | 7.3 | 0.8 |
| $0.5_1^{IV}$ | $Cc$ | 0.59 | 1.2 | 6.9 | 0.8 |
| $0.5_1^V$ | $Pm$ | 0.63 | 0.0 | 0.0 | 0.0 |
| $0.5_2^V$ | $Pm$ | 0.61 | 2.2 | 6.3 | 0.7 |
| PTO | $P4mm$ | 0.87 | 1.3 | 5.2 | 4.4 |

### Summary and conclusions

In this work we have applied random *ab initio* structure searching coupled with the Density Functional Theory methods to describe the structure of Zr-rich PZT ($x$=0.4) using multiphase approach. Our structure searching results demonstrate that the permutation of B-site cations leads to stabilisation of the variety of local phases reflecting a relatively flat energy landscape of PZT in vicinity of the MPB.

We have developed a fitting procedure to reproduce the experimental pair distribution function (PDF) profile using a set of predicted local phases with a high accuracy. We introduce a complex multiphase picture of PZT structure and show that additional monoclinic and rhombohedral phases account for better description of the experimental PDF profile. We propose that at the local scale PZT consists of low-symmetry structures, while macroscopically it belongs to **R** symmetry. This, confirmed by stereographic projection of lead displacements in the model structure, demonstrates random character of distribution of individual directions belonging to monoclinic or triclinic structures around the R-direction. We assume that the origin of such a phase diversity reflects the variety of B-cation arrangements established in the sample during preparation process.

The developed fitting procedure coupled with the *ab initio* random structure searching algorithm [26] for a multiphase structure description is beneficial for applications where structural identification and phase composition, required for characterisation of technologically important macroscopic properties of the material, can be accurately determined through structural property correlations.

This approach, in particular, could provide an insight into the structural definition of complex multiphase, functional ceramics (as electrocaloric, piezoelectric, magnetoelectric compounds); materials with dopants that display fractional site-occupancy; compounds that exhibit degradation of properties or fatigue due to the formation of ad-phase, or phase separation.

The computed parameters of electro-mechanical response show their strong dependence on the symmetry and structural parameters of the local phase. We have not found particularly high piezoelectric coefficients from local phases contributing to $g_m^{PZT}(r)$ including monoclinic ones, which suggests that the *extrinsic* contributions such as domain wall motion are more likely to be responsible for the piezo-activity of PZT rather than the effects of local arrangement.

We hope that some of the considerations, derived in our theoretical investigation, will contribute to a deeper understanding of the experimentally observed phenomena and development of material with desired properties.

**Acknowledgements** Authors are thankful to Dr. N.Zhang and Prof. M.Glazer for experimental data provided. Authors also grateful R. Cohen, M. Cain, J. Jones for fruitful discussions.

This work was funded through the European Metrology Research Programme (EMRP) Project IND54 Nanostrain. The EMRP is jointly funded by the EMRP participating countries within EURAMET and the European Union.

A.K. acknowledges financial support from the European Union's Horizon2020 research and innovation programme within the PETMEM project (Grant 688282). C.J.P. acknowledges financial support from a Royal Society Wolfson Research Merit Award. Via our membership of the UK's HPC Materials Chemistry Consortium, which is funded by EPSRC (EP/L000202), this work made use of the facilities of HECToR and ARCHER, the UK's national high-performance computing service, which is funded by the Office of Science and Technology through EPSRC's High End Computing Programme.

Authors acknowledge facilities of Information and Computing Center of NSU as well as HPC cluster "Academician V.M. Matrosov" at Irkutsk Supercomputer Centre of SB RAS and "Academician V.A. Fock" supercomputer at Irkutsk National Research Technical University.

* anna.kimmel@npl.co.uk

[1] P. Muralt, M. Kohli, T. Maeder, A. Kholkin, K. Brooks, N. Setter and R. Luthier, *Sensors and Actuators A: Physical*, 1995, **48**, 157.
[2] R. Moazzami, C. Hu and W. H. Shepherd, *IEEE Transactions on Electron Devices*, 1992, **39**, 2044.
[3] G. H. Haertling, *Journal of the American Ceramic Society*, 1999, **82**, 797.
[4] J. F. Scott, K. Watanabe, A. J. Hartmann and R. N. Lamb, *Ferroelectrics*, 1999, **225**, 83.
[5] A. Roelofs, T. Schneller, K. Szot and R. Waser, *Nanotechnology*, 2003, **14**, 250.
[6] S. Trolier-McKinstry and P. Muralt, *Journal of Electroceramics*, 2004, **12**, 7.
[7] M. Jeon, H. Chung, K. Kim, K. Oh and S. Woo, *Thin Solid Films*, 2005, **489**, 1.
[8] B. Noheda, D. E. Cox, G. Shirane, J. A. Gonzalo, L. E. Cross and S.-E. Park, *Applied Physics Letters*, 1999, **74**, 2059.
[9] G. Shirane, R. Pepinsky and B. C. Frazer, *Phys. Rev.*, 1955, **97**, 1179.
[10] O. Gindele, A. Kimmel, M. G. Cain and D. Duffy, *The Journal of Physical Chemistry C*, 2015, **119**, 17784.
[11] D. Phelan, X. Long, Y. Xie, Z.-G. Ye, A. M. Glazer, H. Yokota, P. A. Thomas and P. M. Gehring, *Phys. Rev. Lett.*, 2010, **105**, 207601.
[12] A. M. Glazer, P. A. Thomas, K. Z. Baba-Kishi, G. K. H. Pang and C. W. Tai, *Phys. Rev. B*, 2004, **70**, 184123.
[13] N. Zhang, H. Yokota, A. M. Glazer, Z. Ren, D. Keen, D. S. A. Keeble, P. A. Thomas and Z.-G. Ye, *Nat Commun*, 2014, **5**, 5231.
[14] J. Frantti, Y. Fujioka, A. Puretzky, Y. Xie, Z.-G. Ye and A. M. Glazer, *Journal of Applied Physics*, 2013, **113**, 174104–1.
[15] A. M. Glazer, K. Roleder and J. Dec, *Acta Crystallographica Section B*, 1993, **49**, 846.
[16] L. Bellaiche, A. García and D. Vanderbilt, *Phys. Rev.*

*Lett.*, 2000, **84**, 5427.
[17] R. Guo, L. E. Cross, S.-E. Park, B. Noheda, D. E. Cox and G. Shirane, *Phys. Rev. Lett.*, 2000, **84**, 5423.
[18] D. L. Corker, A. M. Glazer, R. W. Whatmore, A. Stallard and F. Fauth, *Journal of Physics: Condensed Matter*, 1998, **10**, 6251.
[19] J. Ricote, D. L. Corker, R. W. Whatmore, S. A. Impey, A. M. Glazer, J. Dec and K. Roleder, *Journal of Physics: Condensed Matter*, 1998, **10**, 1767.
[20] W. Dmowski, T. Egami, L. Farber and P. K. Davies, *AIP Conference Proceedings*, 2001, **582**, 33.
[21] B. Noheda, L. Wu and Y. Zhu, *Phys. Rev. B*, 2002, **66**, 060103.
[22] D. Mao, E. J. Walter, H. Krakauer and Z. Wu, *Phys. Rev. B*, 2007, **76**, 014105.
[23] A. Baldwin, P. A. Thomas and R. Dupree, *Journal of Physics: Condensed Matter*, 2005, **17**, 7159.
[24] D. Vanderbilt and M. H. Cohen, *Phys. Rev. B*, 2001, **63**, 094108.
[25] The $M_c$ phase has $Pm$ symmetry and exhibits polarisation direction of [0uv], where 0<v,u>1, while $M_a$ and $M_b$ both belong to $Cm$ group and are characterised by the polarisation direction of [uuv], with u<v and u>v, respectively. In this notations the $Cm$ phase, identified earler in ref. [8], is $M_a$ type. Similarly, it was shown that at low temperatures this phase transforms to $Cc$ symmetry adopting octahedral rotations [21].
[26] C. J. Pickard and R. J. Needs, *Nature Materials*, 2010, **9**, 624.
[27] We appreciate Nan Zhang, Hiroko Yokota and Mike Glazer for providing us the original neutron data.
[28] I. Grinberg, V. R. Cooper and A. M. Rappe, *Phys. Rev. B*, 2004, **69**, 144118.
[29] C. J. Pickard and R. J. Needs, *Physical Review Letters*, 2006, **97**, 045504.
[30] C. J. Pickard and R. J. Needs, *Journal of Physics: Condensed Matter*, 2011, **23**, 053201.
[31] G. Schusteritsch and C. J. Pickard, *Physical Review B*, 2014, **90**, 035424.
[32] A. J. Bell, *Journal of Materials Science*, 2006, **41**, 13.
[33] J. P. Perdew, A. Ruzsinszky, G. I. Csonka, O. A. Vydrov, G. E. Scuseria, L. A. Constantin, X. Zhou and K. Burke, *Phys. Rev. Lett.*, 2008, **100**, 136406.
[34] G. Kresse and J. Hafner, *Phys. Rev. B*, 1993, **47**, 558.
[35] G. Kresse and J. Hafner, *Phys. Rev. B*, 1994, **49**, 14251.
[36] G. Kresse and J. Furthmüller, *Computational Materials Science*, 1996, **6**, 15.
[37] G. Kresse and J. Furthmüller, *Phys. Rev. B*, 1996, **54**, 11169.
[38] K. Lejaeghere, G. Bihlmayer, T. Björkman, P. Blaha, S. Blügel, V. Blum, D. Caliste, I. E. Castelli, S. J. Clark, A. Dal Corso, S. de Gironcoli, T. Deutsch, J. K. Dewhurst, I. Di Marco, C. Draxl, M. Dułak, O. Eriksson, J. A. Flores-Livas, K. F. Garrity, L. Genovese, P. Giannozzi, M. Giantomassi, S. Goedecker, X. Gonze, O. Grånäs, E. K. U. Gross, A. Gulans, F. Gygi, D. R. Hamann, P. J. Hasnip, N. A. W. Holzwarth, D. Iuşan, D. B. Jochym, F. Jollet, D. Jones, G. Kresse, K. Koepernik, E. Küçükbenli, Y. O. Kvashnin, I. L. M. Locht, S. Lubeck, M. Marsman, N. Marzari, U. Nitzsche, L. Nordström, T. Ozaki, L. Paulatto, C. J. Pickard, W. Poelmans, M. I. J. Probert, K. Refson, M. Richter, G.-M. Rignanese, S. Saha, M. Scheffler, M. Schlipf, K. Schwarz, S. Sharma, F. Tavazza, P. Thunström, A. Tkatchenko, M. Torrent, D. Vanderbilt, M. J. van Setten, V. Van Speybroeck, J. M. Wills, J. R. Yates, G.-X. Zhang and S. Cottenier, *Science*, 2016, **351**, aad300–1.
[39] P. E. Blöchl, *Phys. Rev. B*, 1994, **50**, 17953.
[40] G. Kresse and D. Joubert, *Phys. Rev. B*, 1999, **59**, 1758.
[41] M. Sepliarsky, S. R. Phillpot, S. K. Streiffer, M. G. Stachiotti and R. L. Migoni, *Applied Physics Letters*, 2001, **79**, 4417.
[42] R. W. Nunes and X. Gonze, *Phys. Rev. B*, 2001, **63**, 155107.
[43] I. Souza, J. Íñiguez and D. Vanderbilt, *Phys. Rev. Lett.*, 2002, **89**, 117602.
[44] S. Baroni, P. Giannozzi and A. Testa, *Phys. Rev. Lett.*, 1987, **58**, 1861.
[45] K. Yamasaki, Y. Soejima and K. F. Fischer, *Acta Crystallographica Section B*, 1998, **54**, 524.
[46] S. Aoyagi, Y. Kuroiwa, A. Sawada, H. Tanaka, J. Harada, E. Nishibori, M. Takata and M. Sakata, *Journal of the Physical Society of Japan*, 2002, **71**, 2353.
[47] J. Íñiguez, M. Stengel, S. Prosandeev and L. Bellaiche, *Phys. Rev. B*, 2014, **90**, 220103.
[48] H. Fu and R. Cohen, *Nature*, 2000, **403**, 281.
[49] R. G. Burkovsky, Y. A. Bronwald, A. V. Filimonov, A. I. Rudskoy, D. Chernyshov, A. Bosak, J. Hlinka, X. Long, Z.-G. Ye and S. B. Vakhrushev, *Phys. Rev. Lett.*, 2012, **109**, 097603.
[50] D. Berlincourt and H. H. A. Krüger, *Journal of Applied Physics*, 1959, **30**, 1804.
[51] G. Sághi-Szabó, R. E. Cohen and H. Krakauer, *Phys. Rev. B*, 1999, **59**, 12771.
[52] D. Damjanovic, *Journal of the American Ceramic Society*, 2005, **88**, 2663.